

## REPORTS

plexes, which use small RNAs as guides to target specific mRNAs for degradation or translational repression, we propose that RITS uses siRNAs to recognize and to bind to specific chromosome regions so as to initiate heterochromatic gene silencing (Fig. 5). Four lines of evidence support this view. First, RITS contains Ago1, the *S. pombe* homolog of the Argonaute family of proteins, which form the common subunit of RISC complexes purified from different organisms and are thought to be directly responsible for target recognition (12). Second, RITS is associated with siRNAs that require Dcr1 for their formation and originate from heterochromatin repeat regions. Thus, this complex contains the expected specificity determinants, i.e., siRNAs, which in other systems have been shown to direct target recognition (14, 15, 23, 24). Third, at least two subunits of the RITS complex, Chp1 and Tas3, are specifically associated with the expected heterochromatic DNA regions, which suggests that the complex localizes directly to its target DNA. Fourth, in addition to Ago1, RITS contains a chromodomain protein, Chp1, which is localized throughout heterochromatic DNA regions (18) (Fig. 4) and requires the methyltransferase Ctr4 and histone H3-K9 methylation for localization to chromatin (3, 18). Thus, RITS contains both a subunit (Ago1) that binds to siRNAs and can function in RNA or DNA targeting by sequence-specific pairing interaction and a subunit (Chp1) that associates with specifically modified histones and may be involved in further stabilizing its association with chromatin (Fig. 5).

Mechanisms analogous to the RITS-mediated targeting of heterochromatin complexes are likely to be conserved in other systems. For example, in *Tetrahymena*, genomewide DNA elimination during macronucleus development requires an Argonaute family protein, Twi1, and a chromodomain protein, Pdd1, both of which are also required for H3-K9 methylation and accumulation of small RNAs corresponding to target sequences (8, 25). Similarly, in *Drosophila* repeat-induced transcriptional gene silencing requires an Argonaute family protein, Piwi, and a chromodomain protein, Polycomb (7). Our results support the hypothesis that Argonaute proteins form the core subunit of a number of different effector complexes that use sequence-specific recognition to target either RNA or DNA.

### References and Notes

1. S. I. S. Grewal, *J. Cell. Physiol.* **184**, 311 (2000).
2. S. I. S. Grewal, D. Moazed, *Science* **301**, 798 (2003).
3. J. F. Partridge, K. S. Scott, A. J. Bannister, T. Kouzarides, R. C. Allshire, *Curr. Biol.* **12**, 1652 (2002).
4. D. Zilberman, X. Cao, S. E. Jacobsen, *Science* **299**, 716 (2003).
5. M. Matzke, A. J. M. Matzke, J. M. Kooter, *Science* **293**, 1080 (2001).
6. F. E. Vaistij, L. Jones, D. C. Baulcombe, *Plant Cell* **14**, 857 (2002).
7. M. Pal-Bhadra, U. Bhadra, J. A. Birchler, *Mol. Cell* **9**, 315 (2002).

8. K. Mochizuki, N. A. Fine, T. Fujisawa, M. A. Gorovsky, *Cell* **110**, 689 (2002).
9. T. A. Volpe *et al.*, *Science* **297**, 1833 (2002).
10. I. M. Hall *et al.*, *Science* **297**, 2232 (2002).
11. A. Fire *et al.*, *Nature* **391**, 806 (1998).
12. G. J. Hannon, *Nature* **418**, 244 (2002).
13. P. D. Zamore, *Science* **296**, 1265 (2002).
14. S. M. Hammond, S. Boettcher, A. A. Caudy, R. Kobayashi, G. J. Hannon, *Science* **293**, 1146 (2001).
15. G. Hutvagner, P. D. Zamore, *Science* **297**, 2056 (2002).
16. B. J. Reinhart, D. P. Bartel, *Science* **297**, 1831 (2002).
17. V. Schramke, R. Allshire, *Science* **301**, 1069 (2003).
18. J. F. Partridge, B. Borgstrom, R. C. Allshire, *Genes Dev.* **14**, 783 (2000).
19. G. Thon, J. Verheijen-Hansen, *Genetics* **155**, 551 (2000).
20. C. L. Doe *et al.*, *Nucleic Acids Res.* **26**, 4222 (1998).
21. G. D. Shankaranarayana, M. R. Motamedi, D. Moazed, S. I. S. Grewal, *Curr. Biol.* **13**, 1240 (2003).
22. Materials and methods are available as supporting material on *Science* Online.
23. D. S. Schwarz, G. Hutvagner, B. Haley, P. D. Zamore, *Mol. Cell* **10**, 537 (2002).
24. J. Martinez, A. Patkaniowska, H. Urlaub, R. Luhrmann, T. Tuschl, *Cell* **110**, 563 (2002).
25. S. D. Taverna, R. S. Coyne, C. D. Allis, *Cell* **110**, 701 (2002).
26. J. Nakayama, J. C. Rice, B. D. Strahl, C. D. Allis, S. I. S. Grewal, *Science* **292**, 110 (2001).
27. We thank M. Ohi, K. Gould, C. Hoffman, and D. Wolf for gifts of strains and plasmids; members of the Moazed, Grewal, and Reed laboratories for support and encouragement; R. Ohi and El C. Ibrahim for advice; El C. Ibrahim and M. Wahi for comments on the manuscript; and C. Centrella for technical help. A.V. was supported by a postdoctoral fellowship from INSERM and is now a fellow of the Human Frontier Science Programme. This work was supported by grants from the NIH (S.I.S.G. and D.M.) and a Carolyn and Peter S. Lynch Award in Cell Biology and Pathology (D.M.). D.M. is a scholar of the Leukemia and Lymphoma Society.

### Supporting Online Material

www.sciencemag.org/cgi/content/full/1093686/DC1

Materials and Methods

Figs. S1 to S4

Tables S1 and S2

14 November 2003; accepted 5 December 2003

Published online 2 January 2004;

10.1126/science.1093686

Include this information when citing this paper.

# Kinesin Walks Hand-Over-Hand

Ahmet Yildiz,<sup>1</sup> Michio Tomishige,<sup>3\*</sup> Ronald D. Vale,<sup>3</sup>  
Paul R. Selvin<sup>1,2†</sup>

Kinesin is a processive motor that takes 8.3-nm center-of-mass steps along microtubules for each adenosine triphosphate hydrolyzed. Whether kinesin moves by a "hand-over-hand" or an "inchworm" model has been controversial. We have labeled a single head of the kinesin dimer with a Cy3 fluorophore and localized the position of the dye to within 2 nm before and after a step. We observed that single kinesin heads take steps of  $17.3 \pm 3.3$  nm. A kinetic analysis of the dwell times between steps shows that the 17-nm steps alternate with 0-nm steps. These results strongly support a hand-over-hand mechanism, and not an inchworm mechanism. In addition, our results suggest that kinesin is bound by both heads to the microtubule while it waits for adenosine triphosphate in between steps.

Conventional kinesin (referred to simply as kinesin) is a highly processive, dimeric motor that takes 8.3-nm steps along microtubules (1–3). Kinesin transports a variety of cargo, including membranous organelles, mRNA, intermediate filaments, and signaling molecules (4). Mutations in a neuron-specific conventional kinesin have been linked to neurological diseases in humans (5).

Kinesin is a homodimer with identical catalytic cores (heads) that bind to microtubules and adenosine triphosphate (ATP) (6). Each head is connected to a "neck-linker," a mechanical element that undergoes nucleotide-dependent conformational changes that enable motor stepping (7). The neck linker is in turn connected to a coiled coil that then leads to the cargo-binding

domain (8). In order to take many consecutive steps along the microtubule without dissociating, the two heads must operate in a coordinated manner, but the mechanism has been controversial. Two models have been postulated: the hand-over-hand "walking" model in which the two heads alternate in the lead (7), and an inchworm model in which one head always leads (9).

The hand-over-hand model predicts that, for each ATP hydrolyzed, the rear head moves twice the center of mass, whereas the front head does not translate. For a single dye on one head of kinesin, this leads to a prediction of alternating 16.6-nm and 0-nm translation of the dye (Fig. 1A). In contrast, the inchworm model predicts a uniform translation of 8.3 nm for all parts of the motor, which is equal to the center-of-mass translation (Fig. 1A). In addition, each model makes predictions about rotation of the stalk. The inchworm model predicts that the stalk does not rotate during a step. A symmetric version of the hand-over-hand model, in which the kinesin-microtubule complex is structurally identical at the beginning of each ATP cycle, predicts that the stalk rotates 180 degrees, whereas an asymmetric hand-over-hand

<sup>1</sup>Center for Biophysics and Computational Biology,

<sup>2</sup>Physics Department, University of Illinois, Urbana-Champaign, IL 61801, USA.

<sup>3</sup>Howard Hughes Medical Institute and the Department of Cellular and Molecular Pharmacology, University of California, San Francisco, CA 94107, USA.

\*Present address: Department of Applied Physics, The University of Tokyo, Tokyo 113–8656, Japan.

†To whom correspondence should be addressed. E-mail: selvin@uiuc.edu

model does not require stalk rotation (9, 10). Based on biophysical measurements that showed no rotation of the stalk, Hua *et al.* (9) concluded that an inchworm model was more likely for kinesin, although they could not rule out an asymmetric hand-over-hand mechanism.

Recently, we have developed a technique, Fluorescence Imaging One-Nanometer Accuracy (FIONA), that is capable of tracking the position of a single dye with nanometer accuracy and subsecond resolution (11). In FIONA, the position of a dye before and after a step is monitored by imaging the dye's fluorescence onto a charge-coupled detector through a total-internal-reflection fluorescence microscope. The image, or point-spread-function (PSF), is a diffraction-limited spot with a width of  $\sim 280$  nm, but the center of the image, which corresponds to the position of the dye (12), can be located with nanometer accuracy. We previously applied the technique to show that myosin V walks in a hand-over-hand manner, with each head alternating between 74-nm and 0-nm displacements, while the center of mass moves 37 nm (11).

Here, we have performed analogous experiments with a "cys-light" kinesin (7), with a solvent-exposed cysteine inserted on each head for labeling with a Cy3 fluorophore (Fig. 1B) (13). The dye's position was monitored as the kinesin moved on microtubules that were immobilized on a coverslip (13). Three different constructs were used: a homodimer with glutamic acid mutated to cysteine (E215C), a second homodimer with T324C, and a heterodimer with one head lacking solvent-exposed cysteines and the other head containing cysteines at S43C and T324C, which are 2 nm apart (Fig. 1B). Substoichiometric labeling was used for the homodimers, and single quantal bleaching of fluorescence confirmed that only a single dye was present on each kinesin analyzed (fig. S1B). The heterodimer was labeled with an excess of dye and both single- and double-quantal bleaching was observed (13).

In the absence of ATP, kinesins were stationary. In the presence of 340 nM ATP, discrete steps were observed for the three different kinesin constructs (Fig. 2). A total of 354 steps from 35 kinesins were observed. We typically collected 4000 photons per 0.33-s image. Traces from relatively bright kinesins ( $>5000$  photons per image) are shown in Fig. 2; a histogram of 143 steps from 26 molecules is shown in Fig. 3A. The precision of step-size determination was 1.5 to 3 nm, based on measurement of the distance between the average positions of the PSF centers before and after a step (11, 14). The average step size derived from the step-size histogram (Fig. 3A) is  $17.3 \pm 3.3$  nm. We did not observe 8.3-nm steps or odd multiples of 8.3 nm. These data therefore strongly support a hand-over-hand mechanism and not an inchworm mechanism.

The hand-over-hand mechanism predicts that these 17-nm steps alternate with 0-nm steps, which are not directly observable in a graph of

position versus time. However, if the observed 17-nm steps arise from the convolution of two sequential steps (i.e., 17 nm, 0 nm...), then a dwell-time histogram of the number of steps versus step-time duration will be the convolution of two exponential processes (11). This yields the dwell time probability,  $P(t) = tk^2 \exp(-kt)$ , which is zero at  $t = 0$ , rises initially, and then falls, when  $k$  is the stepping rate constant. In contrast, if the 17-nm steps arise from a single process, then the dwell-time histogram would be

expected to yield an exponential decay (the Poisson-distributed rate). The dwell-time histogram of 347 steps for E215C and T324C (Fig. 3B) is well fit by the above convolution function (with  $k = 1.14 \pm 0.03$  steps per s), and not by the single-step decaying function. The rise near  $t = 0$  is not due to instrument artifacts: An exponential process for myosin V stepping (with dyes located to show every step) at very similar rates yields the expected monotonic decay with the same instrument (11). We also have immo-

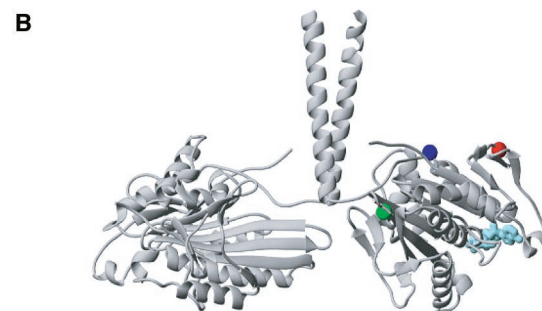
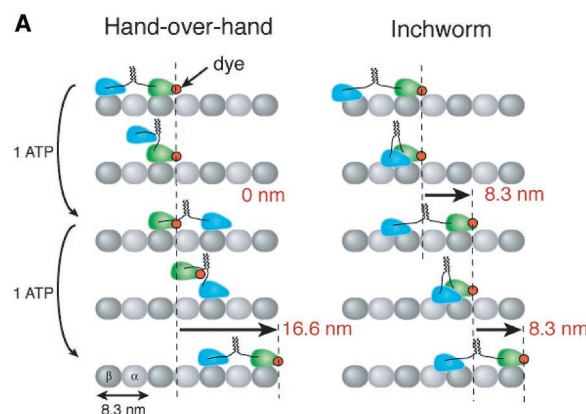


**Fig. 1.** (A) Examples of two alternative classes of mechanisms for processive movement by kinesin. The hand-over-hand model (left) predicts that a dye on the head of kinesin will move alternately 16.6 nm, 0 nm, 16.6 nm, whereas the inchworm mechanism (right) predicts uniform 8.3-nm steps. The inchworm model was adapted with slight modification from (9). (B) The positions of S43 (red), E215 (green), and T324 (blue) on the rat kinesin crystal structure [from (6), Protein Data Base 2KIN]. These residues, whose numbers correspond to conventional human kinesin, were mutated to cysteines for fluorescent dye labeling as described in the text. The bound nucleotide (adenosine diphosphate) is shown as a space-filling model in cyan. This figure was made with MolMol (22).

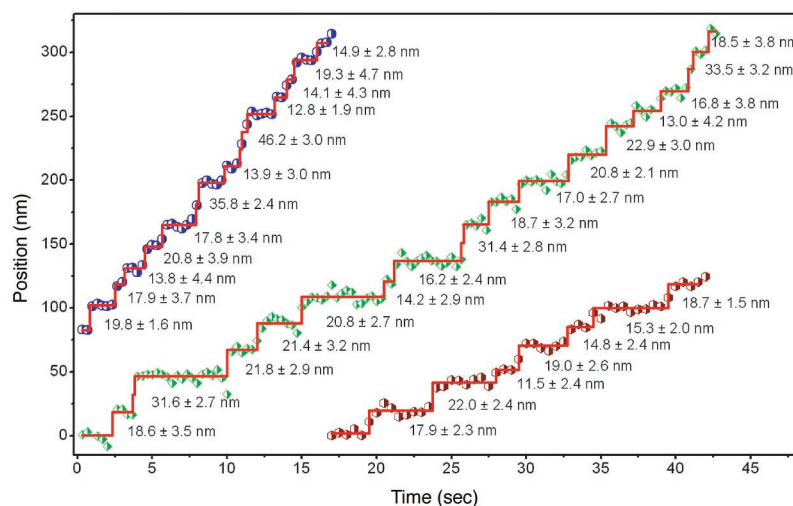


**Fig. 2.** Position versus time for kinesin motility. The blue and green traces are from E215C homodimer kinesin; the red trace, from the heterodimer S43C-T324C kinesin. The numbers correspond to the step size  $\pm \sigma_{\mu}$ . The uncertainties were calculated as described (11). Red lines represent average positions of each duration between steps (plateau) and when the step occurs (jumps) based on data analysis.

## REPORTS

bilized beads on a coverslip and moved them in 17-nm steps with a nanometric stage at the same average step rate and an exponentially distributed dwell time, which yielded the expected dwell-time histogram (fig. S2). The dwell-time histogram therefore provides strong support of the hand-over-hand model.

The average step size of each mutant can also be analyzed and compared. We observed 318 steps from 30 kinesins singly labeled at E215C, and of these, 124 steps from 22 E215C kinesins were chosen for their high-quality images. The average step size was  $17.4 \text{ nm} \pm 3.2 \text{ nm}$  (standard deviation,  $\sigma$ ), with standard error of the mean  $\sigma_{\mu} = 0.3 \text{ nm}$  (Fig. 2, upper left and middle traces, and movie S1). Three T324C kinesins displayed 12 steps with an average step size of  $16.6 \text{ nm} \pm 4.4 \text{ nm}$  ( $\sigma$ ) and  $\sigma_{\mu} = 1.3 \text{ nm}$ . One molecule of S43C-T324C kinesin heterodimer was analyzed (Fig. 2, bottom trace), showing 7 steps with an average step size of  $17.0 \text{ nm} \pm 3.4 \text{ nm}$  and  $\sigma_{\mu} = 1.3 \text{ nm}$ . Consequently, all mutants have an approximately 17-nm average step size, which supports a hand-over-hand model.

Our experiments also have implications for the number of kinesin heads that are bound while kinesin is waiting for ATP. Kinesin is a highly processive motor, implying that at least one head stays bound to the microtubule during multistep motility. Both singly and doubly bound kinesin have been found in the presence of different nucleotides (15, 16), and a two-headed bound species has been inferred to exist during the catalytic cycle based on a kinetic analysis (17) and on fluorescence polarization measurements at saturating ATP concentration (18). However, whether or not kinesin is bound with one or two heads while waiting for ATP during motility has been unclear. If only one head is bound, then the step size would alternate between  $16.6x$  and  $x$ ,

where  $x$  is the distance along the direction of motion from where the dye would be if both heads were bound (fig. S3). We see no evidence for this modulation. For example, the average of every other step of E215C in the upper left trace (Fig. 2, upper left) is  $16.4 \pm 2.9 \text{ nm}$  ( $\sigma_{\mu} = 1.3 \text{ nm}$ ) for the even steps and  $16.9 \pm 3.4 \text{ nm}$  ( $\sigma_{\mu} = 1.5 \text{ nm}$ ) for the odd steps. Similarly, for the green (middle) trace of E215C, the averages are  $17.9 \pm 3.2 \text{ nm}$  ( $\sigma_{\mu} = 1.2 \text{ nm}$ ) for the even steps and  $19.2 \pm 2.9 \text{ nm}$  ( $\sigma_{\mu} = 1.2 \text{ nm}$ ) for the odd steps. Hence, alternating steps are experimentally indistinguishable, indicating that  $x$  is less than 2 nm. Furthermore, in the one-foot-dangling model,  $x$  is expected to be different for each of the different mutants with different dye positions, which again is not observed. Our measurements therefore strongly indicate that the two kinesin heads in the ATP-waiting state are either both bound, or if one head is detached, then it is sitting in a conformation such that it is within 2 nm from a tubulin binding site along the direction of motion.

In conclusion, our results strongly support a hand-over-hand (walking) model for kinesin motility. Combined with the lack of a stalk rotation detected by Hua *et al.* for kinesin (9), our data imply that kinesin moves by an asymmetric hand-over-hand mechanism. Myosin V also walks hand-over-hand (11, 19), although likely not rotating the stalk (20), implying it too is likely asymmetric. Such a mechanism has rather stringent biophysical constraints (9), including implications for how the rear head passes by the front head. Hoenger *et al.* (10) have postulated a model where the rear head passes the front head in such a manner that the neck-linker wraps and unwraps around the stalk with alternating steps to minimize

the build-up of torsional strain in the stalk region. Sideways drag slows the kinesin motor asymmetrically, which suggests left-right asymmetry to the forward-stepping motion and is consistent with, although it does not compel, an asymmetric hand-over-hand model (21). Direct detection of motion during the step, however, requires faster time resolution than presented here.

### References and Notes

1. J. Howard, A. J. Hudspeth, R. D. Vale, *Nature* **342**, 154 (1989).
2. K. Svoboda, C. F. Schmidt, B. J. Schnapp, S. M. Block, *Nature* **365**, 721 (1993).
3. R. D. Vale, R. A. Milligan, *Science* **288**, 88 (2000).
4. L. S. Goldstein, A. V. Philp, *Annu. Rev. Cell Dev. Biol.* **15**, 141 (1999).
5. E. Reid *et al.*, *Am. J. Hum. Genet.* **71**, 1189 (2002).
6. F. Kozielski *et al.*, *Cell* **91**, 985 (1997).
7. S. Rice *et al.*, *Nature* **402**, 778 (1999).
8. R. D. Vale, R. J. Fletterick, *Annu. Rev. Cell Dev. Biol.* **13**, 745 (1997).
9. W. Hua, J. Chung, J. Gelles, *Science* **295**, 844 (2002).
10. A. Hoenger *et al.*, *J. Mol. Biol.* **297**, 1087 (2000).
11. A. Yildiz *et al.*, *Science* **300**, 2061 (2003).
12. For unpolarized dyes, the center of the PSF corresponds to the dye position. For dyes with fixed orientation that emit polarized fluorescence, the PSF can take unusual shapes, particularly when viewed with spherical aberrations, and the PSF center does not necessarily correspond to the dye position (23). In our case, the PSF is well fit to a symmetric two-dimensional Gaussian, implying the center of the PSF corresponds to the dye position. Furthermore, the orientation of the dye in both the hand-over-hand and inchworm models is expected to be unchanged when on the front and rear head, and hence there should be no effect of PSF shape or dye orientation on step-size determination.
13. Materials and methods are available as supporting material on Science Online.
14. The uncertainty, or the standard error of the mean, of the PSF centers for relatively bright spots (5000 photons per image) is  $<3 \text{ nm}$ . Bright spots ( $>7000$  photons per image) yield  $\pm 2 \text{ nm}$  localization of PSF centers (from seven molecules; traces are shown in Fig. 2). We determined the step size by calculating the distance between average positions of plateaus before and after a step. The standard error of the mean of two adjacent plateaus gives the precision of the step size (17).
15. K. Kawaguchi, S. Ishiwata, *Science* **291**, 667 (2001).
16. K. Kawaguchi, S. Uemura, S. Ishiwata, *Biophys. J.* **84**, 1103 (2003).
17. S. S. Rosenfeld, P. M. Fordyce, G. M. Jefferson, P. H. King, S. M. Block, *J. Biol. Chem.* **278**, 18550 (2003).
18. A. B. Asenjo, N. Krohn, H. Sosa, *Nature Struct. Biol.* **10**, 836 (2003).
19. J. N. Forkey, M. E. Quinlan, M. Alexander Shaw, J. E. T. Corrie, Y. E. Goldman, *Nature* **422**, 399 (2003).
20. M. Y. Ali *et al.*, *Nature Struct. Biol.* **9**, 464 (2002).
21. S. M. Block, C. L. Asbury, J. W. Shaevitz, M. J. Lang, *Proc. Natl. Acad. Sci. U.S.A.* **100**, 2351 (2003).
22. R. Koradi, M. Billeter, K. Wüthrich, *J. Mol. Graph.* **14**, 51 (1996).
23. A. P. Bartko, R. M. Dickson, *J. Phys. Chem. B* **103**, 11237 (1999).
24. We thank Y. Oono for helpful discussion of one-versus two-headed binding and the use of fig. S2 and A. Carter for preparing Fig. 1B. Supported by NIH grant nos. AR44420 (P.R.S.) and AR42895 (R.D.V.).

### Supporting Online Material

[www.sciencemag.org/cgi/content/full/1093753/DC1](http://www.sciencemag.org/cgi/content/full/1093753/DC1)  
Materials and Methods  
Figs. S1 to S3  
References and Notes  
Movie S1

17 November 2003; accepted 10 December 2003  
Published online 18 December 2003;  
10.1126/science.1093753  
Include this information when citing this paper.

**Fig. 3.** The step sizes of an individual head of a kinesin dimer and dwell-time analysis support a hand-over-hand mechanism. (A) The kinesin step-size histogram from 124 steps of 22 molecules of E215C, 12 steps of 3 molecules of T324C, and 7 steps of one S43C-T324C heterodimer. The average step size is  $17.3 \pm 3.3 \text{ nm}$  ( $n = 143$ ,  $\sigma_{\mu} = 0.27 \text{ nm}$ ). The black solid line is a Gaussian fit. (B) The dwell-time histogram of 347 steps from 33 kinesin molecules, including 317 steps from 29 molecules of E215C and 30 steps from 4 molecules of T324C, at 340 nM ATP. The black line is a best-fit curve to the convolution function  $tk^2\exp(-kt)$ , with  $k = 1.14 \pm 0.03 \text{ s}^{-1}$  and coefficient of determination  $r^2 = 0.984$ .

